Journal of Biomaterials Applications

IMPROVED CONNECTIVE INTEGRATION OF A DEGRADABLE 3D-NANO-APATITE/AGAROSE SCAFFOLD SUBCUTANEOUSLY IMPLANTED IN A RAT MODEL

Journal:	*Journal of Biomaterials Applications*
Manuscript ID	JBA-18-0230.R1
Manuscript Type:	Original Manuscript
Keywords:	Carbonate-hydroxyapatite, Agarose, Pore architecture, Subcutaneous implant, Tolerance

Abstract: In this work, we evaluate the tissue response and tolerance to a designed 3D porous scaffold composed of nano-carbonate-hydroxyapatite and agarose as a preliminary step in bone repair and regeneration. These scaffolds were subcutaneously implanted into rats, which were sacrificed at different times. CD4+, CD8+ and ED1+ cells were evaluated as measurements of inflammatory reaction and tolerance. We observed some inflammatory response early after subcutaneous implantation. The 3D interconnected porosity increased scaffold integration via the formation of granulation tissue and the generation of a fibrous capsule around the scaffold. The capsule is initially formed by collagen which progressively invades the scaffold, creating a network that supports the settlement of connective tissue and generating a compact structure. The timing of the appearance of CD4+ and CD8+ cell populations is in agreement with the resolved inflammatory response. The appearance of macrophage activity evidences a slow and gradual degradation activity. Degradation started with the agarose component of the scaffold, but the nano-apatite was kept intact for up to 30 days. Therefore, this apatite/agarose scaffold showed a high capacity for integration by a connective network that stabilizes the scaffold and results in slow nano-apatite degradation. The fundamental properties of the scaffold would provide mechanical support and facilitate bone mobilization, which is of great importance in the masticatory system or large bones.

IMPROVED CONNECTIVE INTEGRATION OF A DEGRADABLE 3D-NANO-APATITE/AGAROSE SCAFFOLD SUBCUTANEOUSLY IMPLANTED IN A RAT MODEL

ABSTRACT

In this work, we evaluate the tissue response and tolerance to a designed 3D porous scaffold composed of nano-carbonate-hydroxyapatite and agarose as a preliminary step in bone repair and regeneration. These scaffolds were subcutaneously implanted into rats, which were sacrificed at different times. CD4+, CD8+ and ED1+ cells were evaluated as measurements of inflammatory reaction and tolerance. We observed some inflammatory response early after subcutaneous implantation. The 3D interconnected porosity increased scaffold integration via the formation of granulation tissue and the generation of a fibrous capsule around the scaffold. The capsule is initially formed by collagen which progressively invades the scaffold, creating a network that supports the settlement of connective tissue and generating a compact structure. The timing of the appearance of CD4+ and CD8+ cell populations is in agreement with the resolved inflammatory response. The appearance of macrophage activity evidences a slow and gradual degradation activity. Degradation started with the agarose component of the scaffold, but the nano-apatite was kept intact for up to 30 days. Therefore, this apatite/agarose scaffold showed a high capacity for integration by a connective network that stabilizes the scaffold and results in slow nano-apatite degradation. The fundamental properties of the scaffold would provide mechanical support and facilitate bone mobilization, which is of great importance in the masticatory system or large bones.

Keywords: Carbonate-hydroxyapatite, Agarose, Pore architecture, Subcutaneous implant, Tolerance.

Introduction

In the United States, more than half a million patients per year receive bone defect replacements, costing more than 2.5 billion dollars [1]. Autologous bone is considered the gold standard due to its osteoinductive capacity, the presence of growth factors and osteogenic cells, and its excellent performance as a scaffold that facilitates the viability of osseous implants [2]. However, excessive morbidity, together with availability issues, compromises the use of autologous bone to a great extent. Therefore, allografts and xenografts are feasible alternatives to overcome these complications. However, the use of xenografts is less than ideal due to increased rejection rates and the increased risk of disease transmission due to the use of bovine osseous grafts [3, 4].

Advancements in the development and compatibility of biomaterials are crucial milestones in the progress of tissue engineering and in particular of regenerative medicine. Improvements must especially be geared toward the utilization of biomaterials as substitutes and/or inductors in the repair of different tissues, such as bone. Several studies have demonstrated the validity of such biomaterials as bone substitutes that could decrease patient morbidity while utilizing the most remarkable advantages of autografts: mechanical strength, osteoinduction, osteoconduction and biodegradation [5, 6]. Moreover, to meet the objectives for which these biomaterials were designed, the biomaterials should be properly tolerated by the host organism [6, 7] to avoid long term side effects.

The biomimetic approach, a growing strategy in the biomaterials field, allows the fabrication of materials similar to natural ones, in terms of both composition and structure. For example, apatite, the inorganic component of bones, can be prepared using biomimetic patterning and is an ideal material for osseous regeneration [8]. Moreover, the combination of apatite with natural or synthetic polymers [9-11] deepens this approach and improves its performance.

In this work, scaffolds containing agarose and a nano-carbonate-hydroxyapatite (nCHA) have been prepared by the GELPOR3D [12-14]. This shaping method allows for the preparation of scaffolds that can be described as ceramic reinforced hydrogels. The structural components maintain both their original microstructural and textural properties and thus their original functionality. The ceramic component, apatite crystals of the same order of magnitude as those found in natural bone, facilitates the generation of newly formed bone and improves the mechanical properties of the scaffolds as well

as their handling [15, 16]. The apatite ceramic is embedded in an agarose hydrogel, a three-dimensional polysaccharide matrix that resembles an extracellular matrix where water is the main component. In addition to its many different uses within the biotechnology field [17, 18], agarose is used in the biomaterial field as a matrix to regenerate damaged tissue. It has also been used as a component of a device for controlled drug release. Therefore, agarose has been considered a potential candidate for the regeneration of different types of tissues, especially bone and cartilage [19-24], pancreas [25, 26] and nervous system tissues [27, 28]. Taken together, the combination of both apatite and agarose components constitutes a promising alternative in bone regeneration therapy.

In addition, the possibility of tailoring the pore architecture to mimic that of natural bone tissue should facilitate tissue colonization. This could give rise to a compact composite that would be integrated with soft tissues but would progressively degrade. This would ensure the mechanical support and bone mobilization required in areas such as the masticatory apparatus or large bones. The overall objective of this study was to design a subcutaneous implant model to characterize the tissue tolerance of a designed 3D interconnected porous scaffold composed of nano-carbonate-hydroxyapatite and agarose.

Materials and methods

Fabrication of a 3D macroporous scaffold

The materials used in this work were generated with nanocrystalline carbonate-hydroxyapatite (nCHA), prepared using a precipitation method previously described elsewhere [29], and the polysaccharide agarose (purchased from Sigma-Aldrich). The macroporous nCHA/agarose scaffolds, in an 80/20 weight ratio, were fabricated with a porosity designed using the GELPOR3D method [12-14, 30]. Briefly, a translucent sol was prepared by heating an agarose/water suspension (2.5% wt/vol) at 85ºC; then, the temperature was progressively lowered to approximately 40–45ºC, and the nCHA particles were added under continuous stirring conditions. The obtained slurry was poured into the designed mold, where the suspension gelation process occurred at room temperature within a few minutes. At this point, the pieces were consistent enough to be extracted from the mold, handled and shaped into the desired form. In this study, cylinders 4 mm high and 10 mm in diameter were fabricated. The materials were frozen at -86°C for 24 h and dried in a Heto DRYWINNER lyophilizer for 24 h.

Ectopic implantation of scaffolds

Female Wistar rats (n = 24) between 4-4.5 months of age and with a weight of 235 g ± 15 g were used in this study. This study was carried out in accordance with the European Union guidelines for experimental animal housing and management.

Before the nCHA/agarose biomaterials (4x10 mm) were subcutaneously implanted, they were sterilized using UV radiation for 30 min. The animals were anesthetized with an intraperitoneal injection of ketamine hydrochloride (IMALGENE® 1000 injectable, MERIAL LABORATORIOS, S.A. Barcelona. Spain) and Xilazine hydrochloride (Rompun®, BAYER Barcelona. Spain). To create a pocket for the introduction of the biomaterial piece, a 2 cm incision was created in the skin that covered the dorsal muscle. Finally, the wound was sutured, and the scaffold was enclosed within the subcutaneous cellular tissue (Figure 1). The animals were sacrificed after 7, 14, 21 and 30 days (6 rats per group) by means of an anesthetic overdose. Immediately after the sacrifice, the scaffolds were extracted and prepared for macro and microscopic characterization.

Macroscopic characterization

The wounds were clinically analyzed to detect the presence of edema, flushing, temperature increase, exudate, or any other evidence of inflammation or wound healing alterations. The morphologic characterizations of the implanted scaffolds and the surrounding tissues were performed on randomly selected sections of these areas.

Histology and immunohistochemistry assays

Samples were embedded in paraffin for histological and immunohistochemical studies. Sections (6-8 mm) were extracted from the samples and stained using conventional techniques (Hematoxylin-eosin and Sirius Red stainings for collagen type identification).

The cytotoxicity and biocompatibility studies were performed using immunohistochemistry techniques for the identification of foreign body specific markers as well as the detection of inflammation. The presence of proinflammatory cells (CD4+ and CD8+ lymphocytes) and macrophage cells (ED1+) was determined using immunofluorescence techniques. These studies were performed with a Leica

TCS-SP5 laser confocal microscope using the phycoerythrin and DAPI fluorochromes as tracers to contrast nuclei.

The scaffold angiogenic and osteoinduction capacities were determined using conventional immunohistochemistry techniques. Samples were stained with Vascular Endothelial Growth Factor (VEGF) to determine the angiogenic capacity of the scaffold and Osteopontin (OPN), Osteocalcin (OC), RunX2 and Tartrate Resistant Acid Phosphatase (TRAP) to determine the scaffold osteoinduction capacity.

The following specific monoclonal antibodies were utilized in these assays: Anti-CD4 (LabGen, Germany), 1:50 dilution; Anti-CD8 (LabGen, Germany), 1:50 dilution; Anti-ED1 (Serotec®, UK), 1:100 dilution; Anti-VEGF (ABCam, Cambridge, UK), 1:50 dilution; anti-Osteopontin (Santa Cruz, Madrid, Spain), 1:50 dilution; anti-Osteocalcin (Santa Cruz, Madrid, Spain), 1:50 dilution; anti-RunX2 (Santa Cruz, Madrid, Spain), 1:50 dilution and Anti-TRAP (Santa Cruz, Madrid, Spain), 1:50 dilution.

Statistical Analysis

GraphPad Prism® 5.1 program was used for the statistical analysis, applying the Mann Whitney U test. The significance is set at $p < 0.05$ (*), $p < 0.005$ (**), $p < 0.001$ (***).

Results

nCHA/agarose Scaffolds

The nCHA/agarose scaffolds have been thoroughly characterized in previous studies [13, 14, 30]. The scaffold is macroscopically described as a reinforced hydrogel with a rubber-like texture that can be easily manipulated and shaped by hand by means of a simple cutter. This enables a perfect match of the scaffold into the bone defect. Furthermore, it was determined that the original microstructural characteristics of the nCHA (small size, 15–20 x 3–5 nm, and 8% carbonate content) are maintained after the scaffold fabrication.

The obtained scaffolds displayed a 3D interconnected porosity constituted by “giant” pores approximately 800 μm in size (Figure 1 inset). This porosity was designed to facilitate implant vascularization and cell colonization. The scaffolds possessed a hierarchical pore architecture with additional pore distributions in the 100-200 μm and 50-100 nm ranges that enabled cell migration and fluid exchange. The contribution of these graded pore distributions to the overall porosity, estimated to be approximately 90-95%, could be quantified by means of He pycnometry and Hg intrusion porosimetry. Of the total porosity, 30 ± 0.1% corresponded to the designed giant pores (800 μm),

61.7 ± 0.1% of the porosity was attributed to pores between 100-200 µm generated as a consequence of the freeze-drying process, and the remaining 2.9 ± 0.1% of the porosity was from the pores between 50 and 100 nm that resulted from the spaces that exist between the apatite particles.

The synthesized scaffolds behaved like hydrogel in that the network was able to absorb water or any fluid within its structure, swell without destruction, and maintain its overall architecture. While the overall shape did not change, a slight increase in the scaffold dimensions was observed during the swelling process. This could ensure an ideal fit between the scaffold and the osseous defect.

Subcutaneous implants

Seven days after implantation, the implant zone looked unremarkable and healthy with no evidence of edema or suppuration. This was indicative of a natural healing where the epidermis edges were sealed with normal healing tissue.

Figure 2 shows the macroscopic analysis of the ectopic implants in the subcutaneous layer at different time points. After 7 days of implantation, the scaffold appeared to be surrounded by fibrous tissue with no evidence of rejection or excessive inflammatory reaction (Figure 2a). After 14 days (Figure 2b), the wound scar could hardly be observed, but the implant zone could still be distinguished due to the swelling caused by the biomaterial presence. No inflammatory or suppuration evidence beyond the expected reaction have been detected.

After longer implantation periods of 21 (Fig. 2c) and 30 days (Fig. 2d), there was adequate integration with no foreign body reaction or excessive inflammatory signals. It is important to note the presence of a vascular network around the scaffold capsule, which suggested an optimal tissue response for isolation of the foreign material and a tolerance to drive a slow and clear degradation of this material.

Histology and immunohistochemistry

The optical microscopy studies of the scaffolds that were extracted at different time points and stained with Hematoxylin-eosin are shown in Figure 3. These histological studies allow us to observe the evolution over time of the fibrous capsule (FC) formed around the scaffolds.

Figure 3a shows the microscopy results after 7 days of implantation. At this time, a fibrous reaction is observed; the scaffold appears surrounded by a thin and loose fibrous

capsule. The scaffold insertion zone has closed, and the dermis undergoes a healing process with no evidence of edema formation or presence of inflammatory cells beyond a normal healing process, which is indicative of an absence of foreign body reaction and biomaterial rejection. Fibrous tissues with proliferative fibroblastoid cells were observed within the scaffold pores, whereas several neoformed blood vessels were detected in the implant periphery around the capsule. These observations are evidence of excellent integration and biocompatibility of the scaffold (Figure 3a).

After 14 days of implantation (Figure 3b), the biomaterial is still surrounded by a more fibrous capsule. The input zone has closed, and the dermis is completely healed. The surrounding tissue has colonized the scaffold by penetration within the macropores, where fibroblastoid-shaped cells can be observed. This surrounding tissue is extensively vascularized with several blood vessels around the capsule. The first observation of material resorption can be detected, especially around the lateral edges where an evident thickening of the fibrous capsule can be observed.

After 21 days (Figure 3c), the fibrous capsule starts to stabilize; it is thinner, better organized and more compact than the capsule observed after 14 days. Of note, tissue scaffold colonization occurred in the macropore zone, and vascularization was observed in the capsule periphery. These observations suggest that the biomaterial is starting to become isolated from the subcutaneous tissue with which it had been intimately in contact during the earlier study times. The material resorption is still limited, as the presence of the biomaterial was observed around the lateral edges similar to what was observed after 14 days. Figure 3d shows the scaffold after 30 days of implantation. The capsule becomes thicker, more vascularized, and fibrous around the scaffold. The tissue has completely penetrated within all the macropores, and several cells can be observed inside the biomaterial. This demonstrates successful integration of the biomaterial into the biological tissue. We also observed enhanced material resorption. In addition to the considerable amount of cell colonization in the biomaterial, the absence of edema, foreign body reaction, or giant cells attacking the biomaterial indicated compatibility between the material and the surrounding cell tissue.

The results obtained from Sirius Red staining at different implantation time points are shown in Figure 4. After 7 days, immature collagen (type III) is observed in the implant area around the biomaterial (Figure 4a). No evidence of mature collagen (type I) is detected. The samples extracted after 14 days (Figure 4b) show a more fibrous capsule,

which contains immature collagen, while small zones with collagen type I could be observed.

Figures 4c shows that after 21 days, the expression of mature collagen has increased, especially in the lateral edges around the capsule. After 30 days (Figure 4d), the biomaterial appeared to be completely surrounded by type I mature collagen, especially in some zones of the capsule near the dermis.

The analysis of collagen expression around and inside the scaffold by immunohistochemistry techniques shows no evidence of collagen I markers until 30 days after implantation. At this time, the sample shows a slight increase in expression in some zones of the capsule, specifically those next to the dermis. These observations confirm the results obtained by Sirius Red staining.

There was no evidence of collagen III expression. At the 14 day time point, there was barely distinguishable expression in the tissue that had entered into the biomaterial macropores. However, after 30 days, there is no evidence of this marker.

Immunochemistry characterization was performed using confocal microscopy on the scaffolds at different time points (Figure 5). The presence of CD4+ cells between 7 and 21 days (Figure 5a and 5b, respectively) is more evident when compared to the presence of these cells after 30 days (Figure 5c). At 30 days, expression levels of these markers have decreased, and only a few marked cells can be found within the material. The observation of CD4+ cells reveals the presence of an inflammatory-type reaction in the first 20 days after the implantation. After 30 days, this reaction progressively declines, followed by reabsorption and remodeling of the implant. The location of CD4+ cells depends on the time after implantation: they are observed on the scaffold periphery 21 days after implantation, while after 30 days, the positive cells are located inside the scaffold. Analysis of CD8+ cell expression markers (Figure 5 d-f) demonstrated that hardly any cells were marked after 7 days, while after 21 and 30 days, there was some evidence of CD8+ expression inside the scaffold.

To determine whether the biomaterial is being degraded and whether a cellular reaction from the tissue has been triggered, we characterized the expression of the macrophage marker ED1 at all time points. After 7 and 21 days, there was scarce expression of ED1 in cells located in the capsule area as well as in cells around the material periphery (Figure 5g-h). However, ED1 expression noticeably increases after 30 days (Figure 5i). This is in agreement with the histological characterization of these scaffolds, where an increase in the number of macrophages had been observed. Taken together, our data

indicate that macrophage presence around the scaffold contributed to the degradation of the scaffold.

We next observed that Vascular Endothelial Growth Factor (VEGF) expression was detected after 7 days, and a considerable increase in its expression is observed 21 days after the implantation (Figure 6). VEGF expression was located mostly in the fibrous capsule generated around the scaffold, in the subcutaneous tissue edge opposite to the dermis area.

The highest TRAP expression level was detected after 21 days, and the expression level at 21 days was much higher than at all other time points. After 30 days, decreased TRAP expression was observed. TRAP expression is detected in the cells that have colonized the biomaterial (Figure 7). We then analyzed the expression of the osseous markers Osteopontin (OPN), RunX2 and Osteocalcin (OC) (Figure 8). Expression levels of OPN increased only slightly after 7 days. OPN expression is detected in the tissue area that has penetrated the biomaterial, particularly in the extracellular matrix. There were no RunX2 expressing cells after 7 days; however, after 14 days, we observed low levels of expression of RunX2, which were maintained until 30 days after the implant. RunX2+ cells were detected in the material zone close to the fibrous capsule. Furthermore, OC expression increased after 21 days. All these markers were localized in the extracellular matrix cells of the fibrous capsule included in the giant pores of the scaffold.

Discussion

Apatite and apatite-based biomaterials are excellent candidates for bone repair and regeneration, since apatite is the mineral component of bone and shows an excellent bioactivity, biocompatibility and osteoconductivity [31, 32]. However, it is necessary to analyze the tissue response due to injury at the implantation site. It is also important to note the tolerance capability of the body for acceptance of the foreign body and for the control of the immune system.

In the field of bone tissue engineering, the pore architecture and morphology (microstructure) of the biomaterials to be implanted are critically important, as the pore size (percentage and connectivity) is related to bone formation, high viability, very low mortality and osteoblast proliferation [33]. These material features provide a surface onto which the cells should adhere and grow, while the pore interconnection facilitates

the angiogenic process that is important for the efficient distribution of the neoformed blood vessels within the graft [14, 34].

From a materials perspective, the fabrication method used in this work has allowed the development of scaffolds with a designed composition and architecture. In vitro studies previously performed on human Saos-2 osteoblasts [13] showed no toxicity. This biomaterial allowed the culture of osteoblasts on and around the material without membrane damage, and no oxidative stress was detected.

In our present work in ectopic implants, the macropores of this material facilitate cell intrusion and the production of extracellular matrix within the scaffold, in agreement with results obtained by other studies [35- 37].

This evidence indicates the material degradation of the scaffold while it contributes to the formation of new tissue. Moreover, it has been demonstrated that the pore architecture determines the biomaterial surface area, a critical parameter that ensures a higher surface contact with the surrounding tissues and has a marked influence on the potential release of different substances from the implanted scaffold [38]. A highly connected porous structure may result in significant improvement in bone repair [38]. In our study, the tissue and osteoconduction response obtained for our chosen pore architecture is in agreement with several studies that determined that the ideal pore size for tissue engineering applications should be in the 200-900 μm interval [37]. Therefore, we conclude that the hierarchical pore architecture of the biomaterial studied based on the combination of macropores and micropores is adequate for the generation and integration of neoformed blood vessels within the tissue that colonizes it. Furthermore, other studies suggest that biomaterials based on nano-hydroxyapatite are excellent candidates for hard tissue engineering and that pore size distribution is critical for cellular colonization [39].

Our collagen expression studies reveal that most of the collagen is formed in the capsule that surrounds the biomaterial; in addition, this collagen can be identified as immature (type III) [40] after 7 and 14 days of implantation, while at 30 days, the expressed collagen was identified as type I (mature collagen).

Histological studies confirmed that after 14 days, many neoformed blood vessels were observed not only around the biomaterial but also passing through its macropores. This invasion ensures nutrient arrival and waste elimination, thus facilitating cell survival and new tissue formation. The presence of the blood vessel formation marker VEGF was detected throughout the study, with maximum expression after 21 days. These

results agree with previous studies that showed that the subcutaneous implant of different types of hydroxyapatite-based biomaterials induces the formation of a capsule composed by fibrous tissue, an enhanced vascularization and the presence of multinucleated giant cells [36]. Concerning the immune response, the absence of evident inflammation demonstrates that the scaffold itself, and its degradation products, are not toxic. These results agree with those obtained by using poly(D,L lactide)/nano-hydroxyapatite composite scaffolds [41] where both neutrophils and lymphocytes remain in the tissue 9 weeks after the biomaterial implantation.

The presence of CD4 and CD8 positive cells indicates an inflammatory-type reaction in the first 20 days after the implantation that progressively decreases. Simultaneously, scaffold resorption and bone remodeling were observed, in agreement with increased TRAP expression. Cells that express CD4 were found in the tissue surrounding the material at early stages, thus indicating the usual physiological-defense reaction against the implant. This response is beneficial considering that the activation of the host tissue by the material is required to trigger the regeneration process. The expression of CD4+ cells confirms that the nCHA/agarose scaffold activates a mild immune response that progressively declines over time as can be deduced from the scarce presence of CD4+ cells after 30 days. On the other hand, the expression of the CD8 marker (cytotoxic lymphocytes) is low and decreases to close to zero after 21 days. Therefore, we confirmed that the immune system activation does not induce a rejection reaction against the implant. The balanced presence of both markers demonstrates an adequate reaction from the host tissue to the implanted scaffold. Moreover, Anderson *et al* [42] argue that the presence of foreign body multinucleated giant cells facilitates the material resorption process. Thus, we conclude that the material is being resorbed after 14 days, and cells of this lineage can be detected.

The ED1 marker, specific for rat macrophages, was detected mainly around the scaffold at all time points studied. Although expression of this marker slightly increased with time, no uncontrolled macrophage reactions were observed. After 30 days, the scaffold starts to be gradually resorbed, which agrees with the results of Holzapfel *et al* [43] for hydroxyapatite subcutaneous implantations in humans. These authors observed that after 18 months, residues of the material remained in the implantation site, thus indicating a slow resorption process. The scarce amount of macrophages observed in both their work and in the present work, suggests that scaffolds based on hydroxyapatite are characterized by a slow resorption process and a moderate cell response.

To ascertain if the material used in this work has osteoconductive properties when ectopically implanted, different markers of the osteogenic lineage were analyzed (Figure 8). The low levels of osteopontin expression at all time points suggest that the scaffold degradation may induce matrix formation, which may increase the osteogenic differentiation of the progenitor cells coming from the host tissue. In addition, expression of the TRAP marker is indicative of a remodeling process of the osteoclastic lineage cells. Furthermore, weak expression of Runx2, an early transcription factor within the chondrogenic and osteogenic lineages differentiation reaction, has been detected. In addition, the prominent expression of OC observed is indicative of osteogenic tissue formation as a consequence of the subcutaneous implantation of the nCHA/agarose scaffold.

Conclusion

The present work describes the successful use of an ectopic rat model to study the material resorption and osteoinductive properties of 3D macroporous apatite/agarose scaffolds. The scaffold used in this work shows a satisfactory biocompatibility when implanted subcutaneously. After 30 days, the biomaterial starts to be gradually resorbed, indicating that the material is also biodegradable. Taken together, our data along with other studies concludes that the proposed scaffold fulfills the biological requisites of tissue engineering. Histological and immunochemical studies show that the scaffold is capable of promoting in vivo osteogenesis in ectopic areas. These results support the usefulness of these apatite/agarose scaffolds as a potential material for applications in guided bone regeneration.

It must be highlighted that the chemical composition is not the only factor that has a critical influence on the biocompatibility and biodegradability of these scaffolds. It has been verified that both the microstructure and the hierarchical pore architecture facilitate cell colonization, fluid exchange and implant vascularization.

To summarize, we can conclude that 3D nano-apatite/agarose scaffold improves connective integration while slowing apatite degradation. Thus, this biomaterial would drive rapid bone mobilization.

References

[1] Amini A.R., Laurencin C.T., Nukavarapu S.P. Bone Tissue Engineering: Recent Advances and Challenges. *Critical reviews in biomedical engineering*. 2012. 40(5): 363-408.

[2] Campana V., Milano G., Pagano E., Barba M., Cicione C., Salonna G., Lattanzi W., Logroscino G. Bone substitutes in orthopaedic surgery: from basic science to clinical practice. *Journal of Materials Science: Materials in Medicine*. 2014. 25(10): 2445-2461.

[3]Tommasi G., Perni S., Prokopovich P. An Injectable Hydrogel as Bone Graft Material with Added Antimicrobial Properties. *Tissue engineering. Part A.* 2016. 22(11-12): 862-72.

[4] Kubosch E.J., Bernstein A., Wolf L., Fretwurst T., Nelson K., Schmal H. Clinical trial and in-vitro study comparing the efficacy of treating bony lesions with allografts versus synthetic or highly-processed xenogeneic bone grafts. *BMC musculoskeletal disorders*. 2016.17: 77.

[5] Ripamonti U., Roden L. Biomimetics for the induction of bone formation. *Expert Review of Medical Devices.* 2010. 7(4):469-479.

[6] Noh Y.K., Du P., Kim I.G., Ko J., Kim S.W., Park K. Polymer mesh scaffold combined with cell-derived ECM for osteogenesis of human mesenchymal stem cells. *Biomaterials Research.* 2016.20(1): 6.

[7] Mizuno H. Adipose-derived Stem Cells for Tissue Repair and Regeneration: Ten Years of Research and a Literature Review. *Journal of Nippon Medical School.* 2009.76(2) : 56-66.

[8] Calabrese G., Giuffrida R., Fabbi C., Figallo E., Lo Furno D., Gulino R., Colarossi C., Fullone F., Giuffrida R., Parenti R., Memeo L., Forte S. Collagen-Hydroxyapatite Scaffolds Induce Human Adipose Derived Stem Cells Osteogenic Differentiation In Vitro. *PLoS One*. 2016. 11(3): e0151181.

[9] Ikada Y. Challenges in tissue engineering. *Journal of the Royal Society Interface* . 2006. 3(10): 589-601.

[10] Bleek K., Taubert A. New developments in polymer-controlled, bioinspired calcium phosphate mineralization from aqueous solution. *Acta Biomaterialia.* 2013.9(5) :6283-6321.

[11] Wagoner Johnson A.J., B Herschler.A.b A review of the mechanical behavior of CaP and CaP/polymer composites for applications in bone replacement and repair. *Acta Biomaterialia*. 2011.7(1):16-30.

[12] Peña J., Román J., Victoria Cabañas M., Vallet-Regí M. An alternative technique to shape scaffolds with hierarchical porosity at physiological temperature. *Acta Biomaterialia.* 2010.6(4):1288-1296.

[13] Cabañas M.V., Peña J., Román J., Ramírez-Santillán C., Matesanz M.C., Feito M.J., Portolés M.T., Vallet-Regí M. Design of tunable protein-releasing nanoapatite/hydrogel scaffolds for hard tissue engineering. *Materials Chemistry and Physics.* 2014. 144(3):409-417.

[14] Roman J., Cabanas M.V., Pena J., Vallet-Regi M. Control of the pore architecture in three-dimensional hydroxyapatite-reinforced hydrogel scaffolds. *Science and Technology of Advanced Materials.* 2011. 12(4): 045003.

[15] Vallet-Regi M. Revisiting ceramics for medical applications. *Dalton Transactions*. 2006. 44: 5211-5220.

[16] Vallet-Regí M., González-Calbet J.M. Calcium phosphates as substitution of bone tissues. *Progress in Solid State Chemistry.* 2004. 32(1–2): 1-31.

[17] Renn D.W. Agar and Agarose-Indispensable Partners in Biotechnology. *Industrial & Engineering Chemistry Product Research and Development.* 1984. 23(1): 17-21.

[18] Rinaudo M. Main properties and current applications of some polysaccharides as biomaterials. *Polymer International*. 2008. 57(3): 397-430.

[19] Chung C., Burdick J.A. Engineering cartilage tissue. *Adv. Drug Deliv. Rev.* 2008. 60(2) :243-262.

[20] Khanarian N.T., Haney N.M., Burga R.A., Lu H.H. A functional agarose-hydroxyapatite scaffold for osteochondral interface regeneration. *Biomaterials.* 2012. 33(21): 5247-5258.

[21] Iwai S., Shimizu H., Suzawa Y., Akashi M., Yura Y. Hydroxyapatite agarose composite gels as a biochemical material for the repair of alveolar bone defects due to cleft lip and palate. *Journal of Oral and Maxillofacial Surgery, Medicine, and Pathology.* 2015. 27(5):637-644.

[22] Suzawa Y., Kubo N., Iwai S., Yura Y., Ohgushi H., Akashi M. Biomineral/agarose composite gels enhance proliferation of mesenchymal stem cells with osteogenic capability. *International Journal of Molecular Sciences*. 2015. 16(6):14245-14258.

[23] Mizuta N., Hattori K., Suzawa Y., Iwai S., Matsumoto T., Tadokoro M., Nakano T., Akashi M., Ohgushi H., Yura Y. Mesenchymal stromal cells improve the

osteogenic capabilities of mineralized agarose gels in a rat full-thickness cranial defect model. *Journal of Tissue Engineering and Regenerative Medicine.* 2013.7(1):51-60.

[24] Hu J.-X., Ran J.-B., Chen S., Jiang P., Shen X.-Y., Tong H. Carboxylated Agarose (CA)-Silk Fibroin (SF) Dual Confluent Matrices Containing Oriented Hydroxyapatite (HA) Crystals: Biomimetic Organic/Inorganic Composites for Tibia Repair. *Biomacromolecules.* 2016. 17(7): 2437-2447.

[25] Bloch K., Lozinsky V.I., Galaev I.Y., Yavriyanz K., Vorobeychik M., Azarov D., Damshkaln L.G., Mattiasson B., Vardi P. Functional activity of insulinoma cells (INS-1E) and pancreatic islets cultured in agarose cryogel sponges. *Journal of Biomedical Materials Research Part A* . 2005. 75A (4): 802-809.

[26] Teramura Y., Iwata H. Bioartificial pancreas Microencapsulation and conformal coating of islet of Langerhans. *Adv. Drug Deliv. Rev.* 2010. 62(7-8): 827-840.

[27] Bellamkonda R.V. Peripheral nerve regeneration: An opinion on channels, scaffolds and anisotropy. *Biomaterials.* 2006. 27(19): 3515-3518.

[28] Lynam D.A., Shahriari D., Wolf K.J., Angart P.A., Koffler J., Tuszynski M.H., Chan Walton C., P., Sakamoto J. Brain derived neurotrophic factor release from layer-by-layer coated agarose nerve guidance scaffolds. *Acta Biomaterialia*. 2015. 18(0): 128-131.

[29] Padilla S., Izquierdo-Barba I., Vallet-Regí M. High Specific Surface Area in Nanometric Carbonated Hydroxyapatite. *Chemistry of Materials.* 2008. 20(19): 5942-5944.

[30] Alcaide M., Serrano M.-C., Roman J., Cabañas M.-V., Peña J., Sánchez-Zapardiel E., Vallet-Regí M., Portolés M.-T. Suppression of anoikis by collagen coating of interconnected macroporous nanometric carbonated hydroxyapatite/agarose scaffolds. *Journal of Biomedical Materials Research Part A.* 2010. 95A (3):793-800.

[31] Calasans-Maia M.D., de Melo B.R., Alves A.T.N.N., Resende R.F.d.B., Louro R.S., Sartoretto S.C., Granjeiro J.M., Alves G.G. Cytocompatibility and biocompatibility of nanostructured carbonated hydroxyapatite spheres for bone repair. *Journal of Applied Oral Science.* 2015. 23(6): 599-608.

[32] Shahrezaie M, Moshiri A, Shekarchi B, Oryan A, Maffulli N, Parvizi J. Effectiveness of tissue engineered three dimensional bioactive graft on bone

healing and regeneration: an in vivo study with significant clinical value. *J Tissue Eng Regen Med*, 2017 .doi: 10.1002/term.2510.

[33] Aragon J, Navascues N, Mendoza G, Irusta S. Laser-treated electrospun fibers loaded with nano-hydroxyapatite for bone tissue engineering. *Int J Pharm.* 2017. 525(1):112-122.

[34] Huang J., Xiong, Jiany, Liu, Jianquan, Zhu, Weimin, Chen, Jielin, Duan, Li, Zhang, Jufeng, Wang, Daping. Evaluation of the novel three-dimensional porous poly (L-lactic acid)/nano-hydroxyapatite composite scaffold. *Bio-medical Materials and Engineering*. 2015. 26(Suppl. 1): S197-205.

[35] Zhang J., Xu Q., Huang C., Mo A., Li J., Zuo Y. Biological properties of an anti-bacterial membrane for guided bone regeneration: an experimental study in rats. *Clinical Oral Implants Research*. 2010. 21(3):321-327.

[36] Shahram G., Carina O., Mike B., Ines W., Benjamin W.T., Patrick B., Stefan S., Constantin L., Robert Anton S., Charles James K. Histological and histomorphometrical analysis of a silica matrix embedded nanocrystalline hydroxyapatite bone substitute using the subcutaneous implantation model in Wistar rats. *Biomedical Materials.* 2010 .5(3): 035005.

[37] Vallet-Regi M., Colilla M., Gonzalez B. Medical applications of organic-inorganic hybrid materials within the field of silica-based bioceramics. *Chemical Society Reviews.* 2011. 40(2): 596-607.

[38] Zhang S, Jiang G, Prabhakaran MP, Qin X, Ramakrishna S. Evaluation of electrospun biomimetic substrate surface-decorated with nanohydroxyapatite precipitation for osteoblasts behavior. *Mater Sci Eng C Mater Biol Appl.* 2017. 1: 79:687-696.

[39] Wang T., Yang X., Qi X., Jiang C. Osteoinduction and proliferation of bone-marrow stromal cells in three-dimensional poly (ε-caprolactone)/ hydroxyapatite/collagen scaffolds. *Journal of Translational Medicine.* 2015. 13:152-162.

[40] Liuyun J., Yubao L., Chengdong X. Preparation and biological properties of a novel composite scaffold of nano-hydroxyapatite/chitosan/carboxymethyl cellulose for bone tissue engineering. *Journal of Biomedical Science*. 2009. 16(1): 65-65.

[41] Ren J., Zhao P., Ren T., Gu S., Pan K. Poly (d,l-lactide)/nano-hydroxyapatite composite scaffolds for bone tissue engineering and biocompatibility evaluation. *Journal of Materials Science: Materials in Medicine.* 2008.19(3):1075-1082.

[42] Anderson J.M., Rodriguez A., Chang D.T. Foreign body reaction to biomaterials. *Seminars in Immunology.* 2008. 20(2): 86-100.

[43] Holzapfel A.M., Mangat D.S., Barron D.S. Soft-tissue augmentation with calcium hydroxylapatite: Histological analysis. *Archives of Facial Plastic Surgery*. 2008. 10(5): 335-338.

Figure legends

Figure 1. a) Subcutaneous implant of nCHA/agarose scaffolds in Wistar female rats. Inset: Macroscopic image of the piece introduced. b) Scanning electron microscopy image of the piece introduced.

Figure 2. Photographs of the ectopic implant at different time points: a) 7 days, b) 14 days, c) 21 days and d) 30 days.

Figure 3. Microscopic images, at O.M. 5x, of the stained implants (Hematoxylin-Eosin) at different time points: a) 7 days, b) 14 days, c) 21 and d) 30 days. (S = Skin; FC = Fibrose Capsule; BV = Blood Vessel; CHA = nCHA/Agarose scaffold).

Figure 4. Microscopic images, at O.M. 10x, of the stained implants (Sirius Red) at different time points: a) 7 days, b) 14 days, c) 21 and d) 30 days. (FC = Fibrose Capsule; CHA = nCHA/Agarose scaffold).

Figure 5. Microscopic images, at O.M. 20x, of the implants (Immunofluorescence staining) at different time points CD4+ cells at a) 7 days, b) 21 days and c) 30 days; CD4+ cells at d) 7 days, e) 21 days and f) 30 days; ED1+ cells at g) 7 days, h) 21 days and i) 30 days.

Figure 6. Microscopic images of VEGF immunohistochemical staining (12,5x) at 7 days (a), 14 days (b), 21 days (c), 30 days (d). e) Expression of VEGF+ cells over time (7-30 days) Data are expressed as the % of cells that are VEGF+. Significant differences are detected after 21 and 30 days when compared to earlier time points (*$p<0.05$).

Figure 7. Microscopic images of TRAP immunohistochemical staining: a) Negative control (O.M. 40x); b) 7 days (O.M. 40x); c) 14 days (O.M. 40x); d) 21 days (O.M. 40x); e) 30 days (O.M. 40x); f) Quantification of the percentage of labeled cells at each time point. There was a significant increase in TRAP levels at 21 days, remaining high at 30 days (*p<0,05).

Figure 8. a) Expression of markers for angiogenesis (VEGF), osteogenesis (OPN) and bone remodeling (TRAP) at different time points. (VEGF = Vascular Endothelial Growth Factor; OPN = Osteopontin; TRAP = Resistant Tartrate Acid Phosphatase). (- = no expression, 0-10% marked cells; + = slight expression, 10-35%; ++ = moderate expression, 35-50%; +++ = high expression, > 50%). and Microscopic images of OPN immunohistochemical staining (12,5x) at 7 days (b), 14 days (c), 21 days (d), 30 days (e).

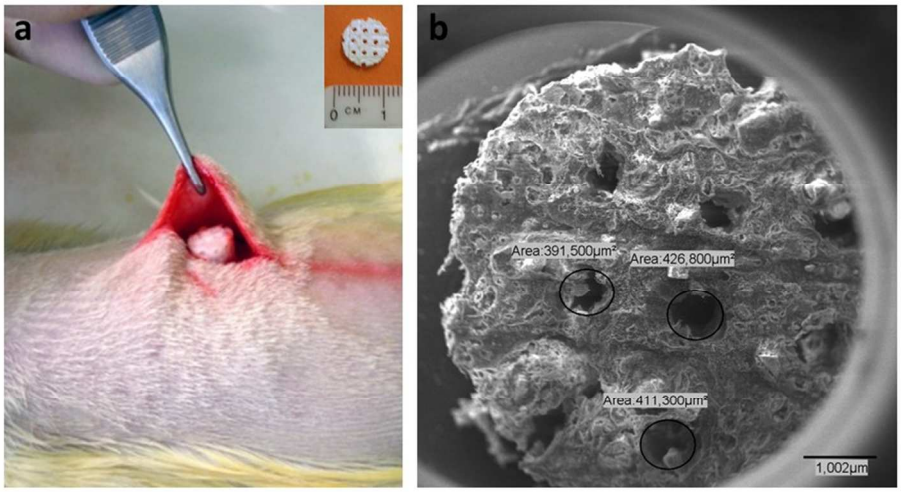

254x190mm (96 x 96 DPI)

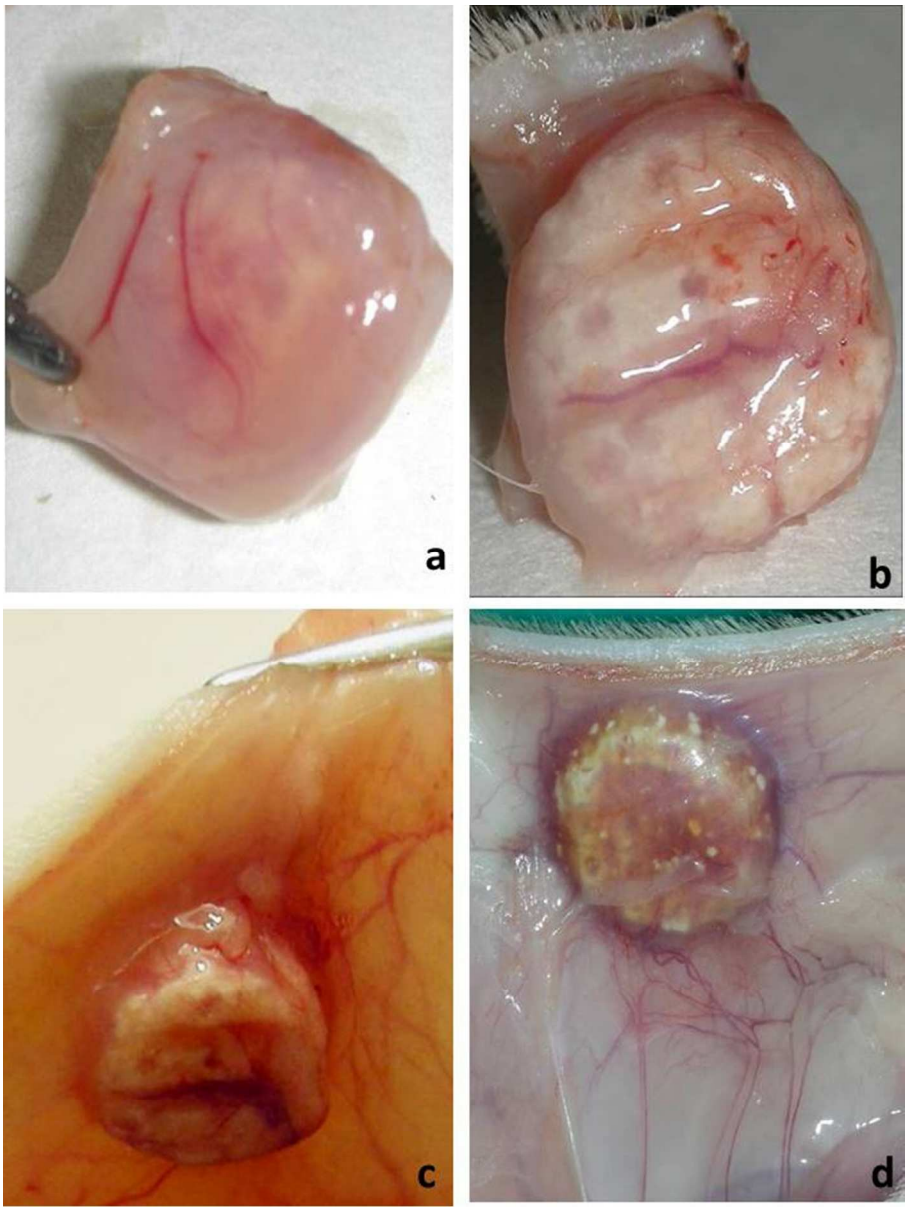

190x254mm (96 x 96 DPI)

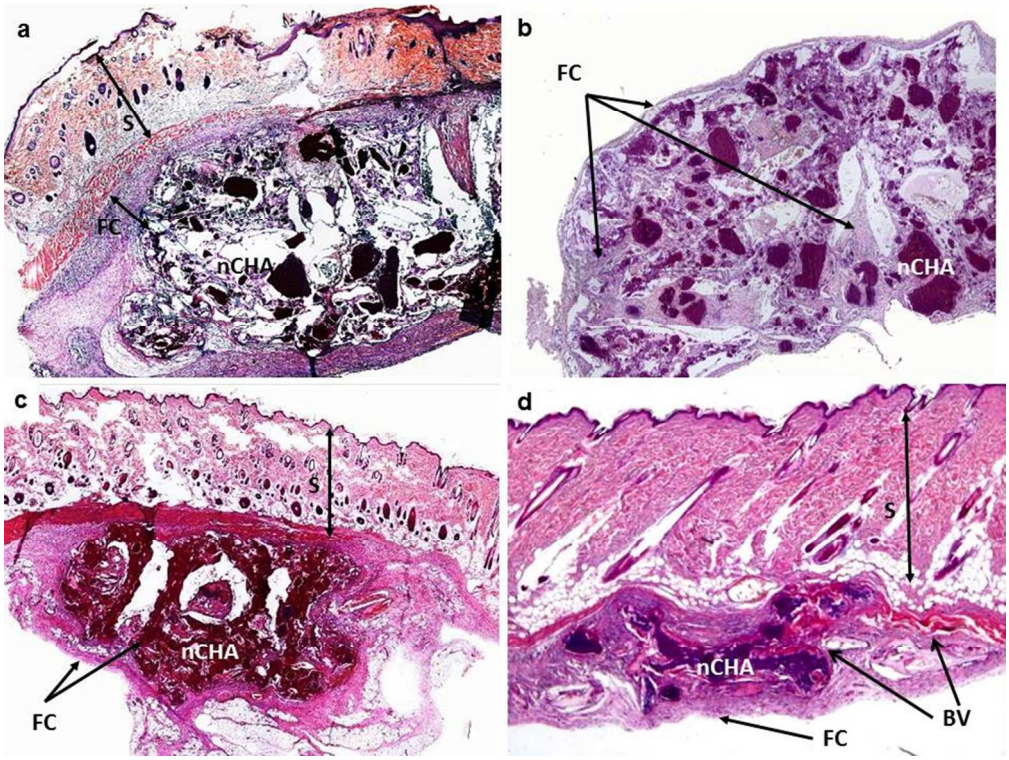

254x190mm (96 x 96 DPI)

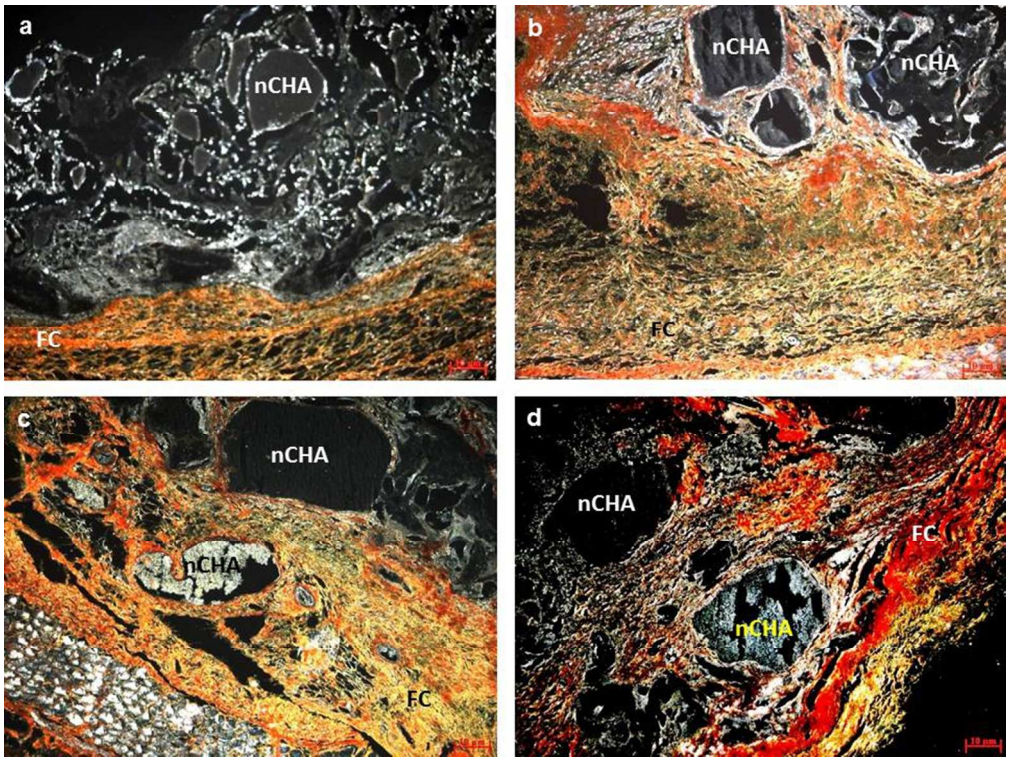

254x190mm (96 x 96 DPI)

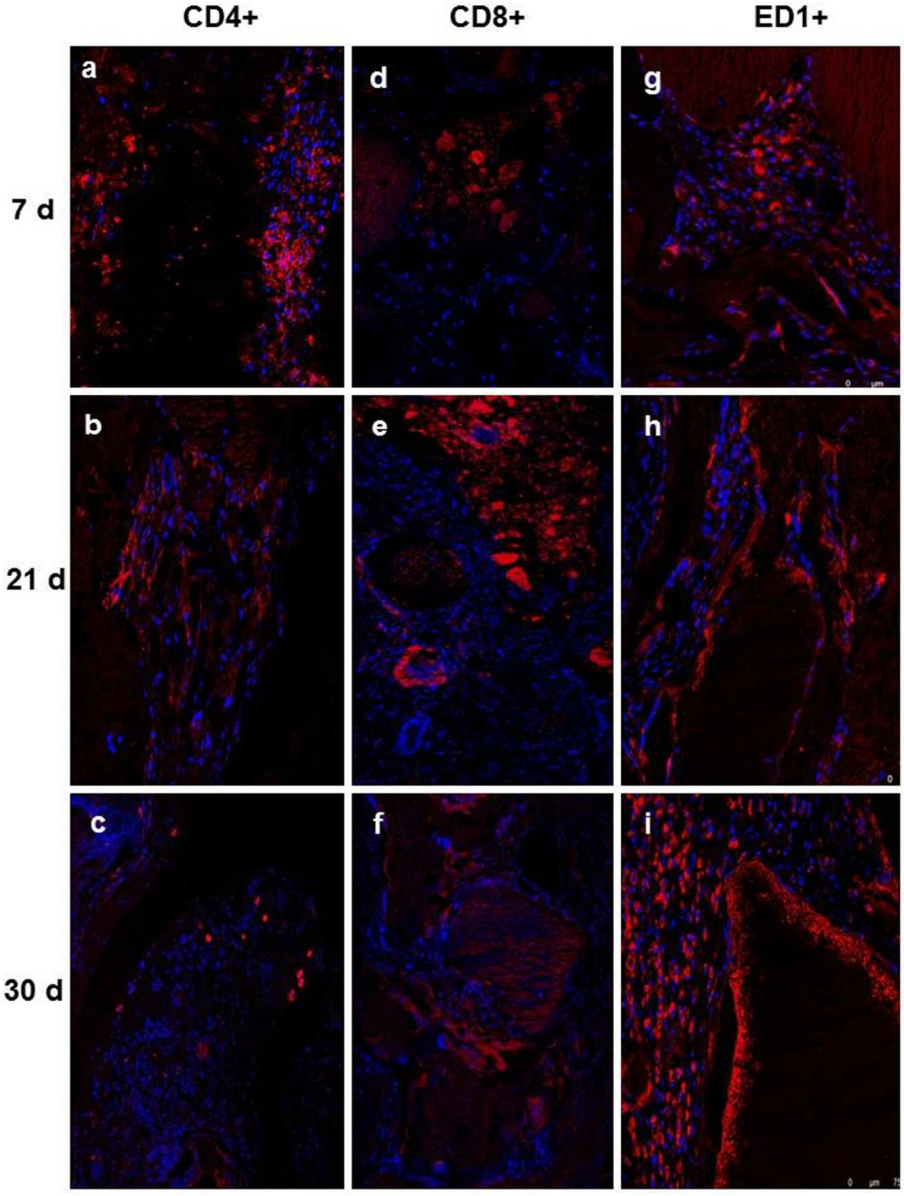

190x254mm (96 x 96 DPI)

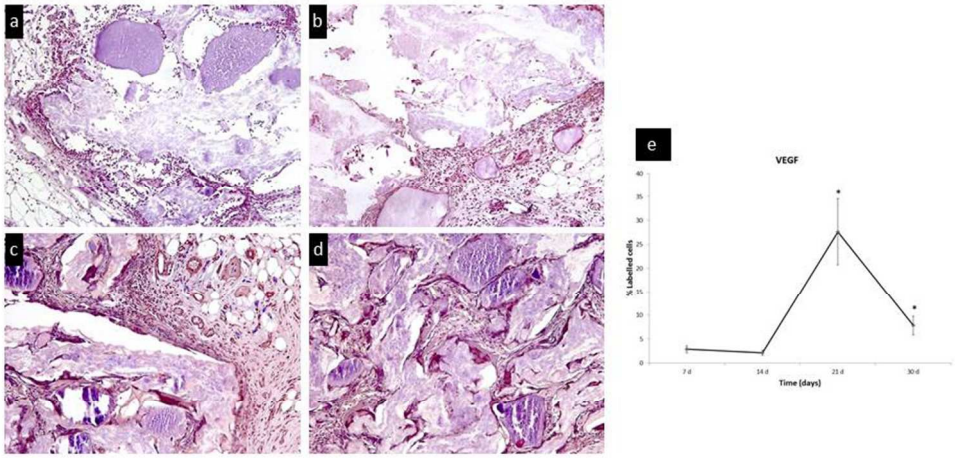

254x190mm (96 x 96 DPI)

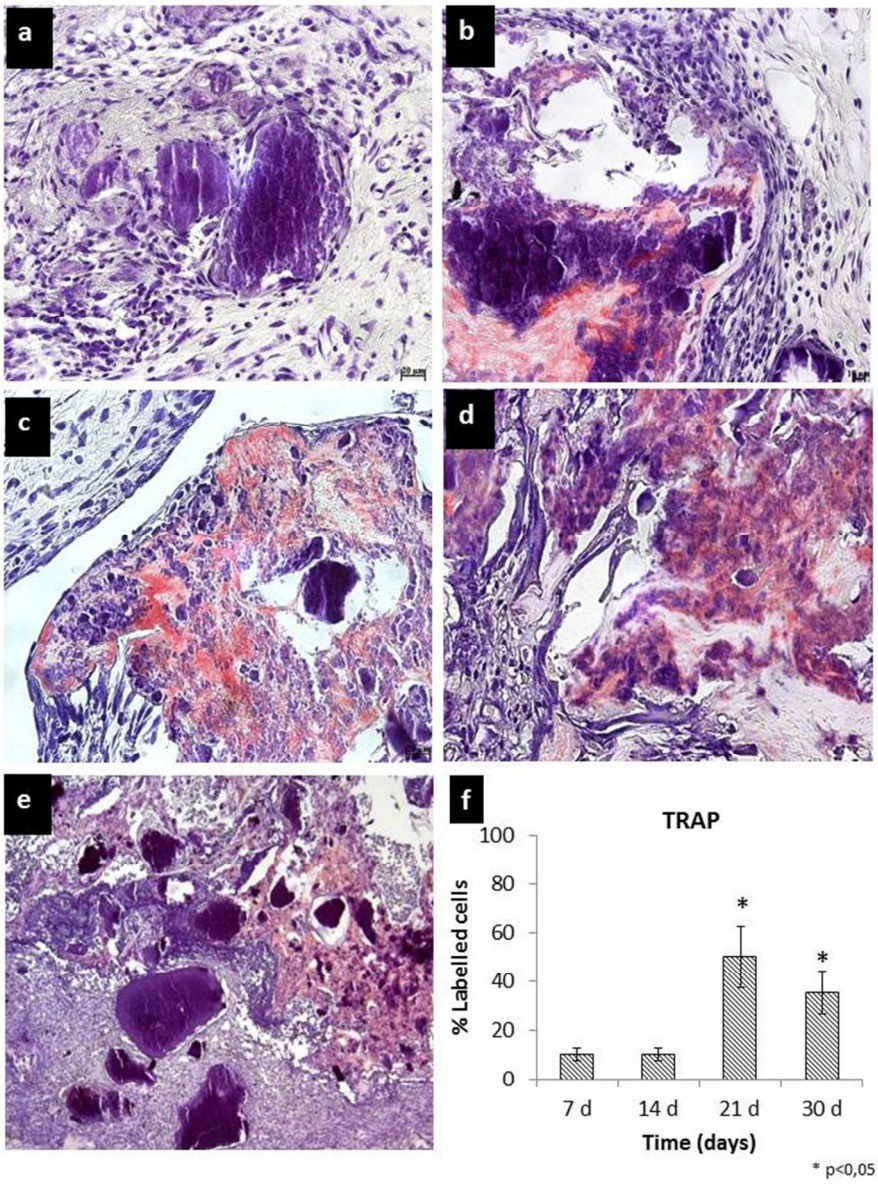

190x254mm (96 x 96 DPI)

a

	VEGF	OPN	TRAP
7 d	-	+++	+
14 d	+	+	+
21 d	+++	+	+++
30 d	++	+	++

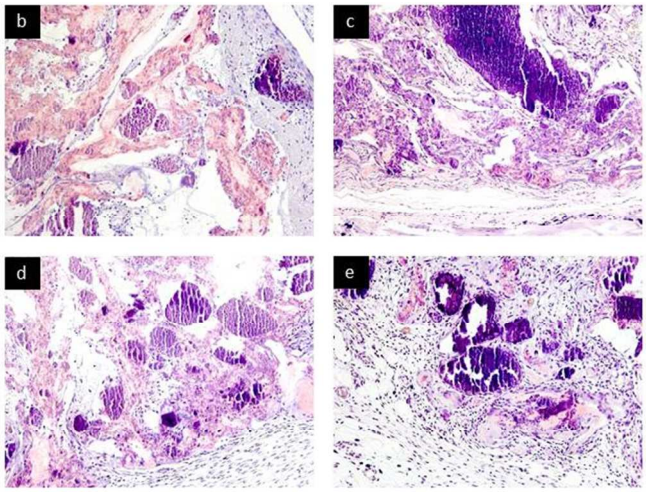

254x190mm (96 x 96 DPI)